energy&fuels

pubs.acs.org/EF Article

Improved Performance and Efficiency of Lanthanum–Strontium–Manganese Perovskites Undergoing Isothermal Redox Cycling under Controlled pH_2O/pH_2

Kangjae Lee, Dylan C. McCord, Richard J. Carrillo, Bella Guyll, and Jonathan R. Scheffe*

Cite This: *Energy Fuels* 2020, 34, 16918–16926 Read Online

ACCESS | Metrics & More | Article Recommendations | Supporting Information

ABSTRACT: Two-step thermochemical redox cycles represent an attractive pathway toward producing solar fuels via H_2O and CO_2 splitting. These cycles typically operate at two different temperatures, but isothermal cycling has been proposed as a means to minimize the sensible heating requirements of the solid phase. Recently, a theoretical analysis showed that lanthanum–strontium–manganese-based perovskites compare favorably to the state-of-the-art material, ceria, when evaluated in the context of isothermal cycling. In this work, a high-temperature reactor system that affords precise control of partial pressures of H_2O and H_2 (pH_2O/pH_2), and thus reduction and oxidation conditions, was utilized for isothermal cycling of ceria, $La_{0.65}Sr_{0.35}MnO_3$ (LSM35) and $La_{0.6}Sr_{0.4}MnO_3$ (LSM40), in order to validate theoretical predictions experimentally. Data are measured between 1300 and 1400 °C and between oxygen partial pressures (pO_2) of 8×10^{-7} atm (reduction, pH_2O/pH_2 in the range of 62.73–203.17) and 5×10^{-5} atm (oxidation, pH_2O/pH_2 in the range of 250.92–507.93). Both LSM35 and LSM40 significantly outperformed ceria while operating isothermally in terms of H_2 production and performance (Π), a new metric introduced in this article. This material-specific metric is related to efficiency, but enables straightforward comparison of materials directly from only a few measured experimental data points. Overall, experimental data agree well with theoretical predictions, giving promise to isothermal operation for this class of materials. Overall, this work provides motivation for material exploration and development of materials that undergo large changes in nonstoichiometry in the pO_2 range between 8×10^{-7} atm and 5×10^{-5} atm. Importantly, because operation is isothermal or near-isothermal, material exploration is not limited to materials possessing large entropic changes similar to those aimed specifically at temperature-swing redox cycling, opening the door to new possibilities and different material classes from those have been considered prior.

INTRODUCTION

Two-step redox cycles utilizing metal oxides such as ceria (CeO_2) and perovskites are capable of splitting H_2O and CO_2 using a high-temperature heat source, such as concentrated solar radiation. These reactions are split into an endothermic reduction step and exothermic oxidation step, expressed as follows for ceria

$$\text{reduction: } CeO_{2-\delta_i} \rightarrow CeO_{2-\delta_f} + (\delta_f - \delta_i)/2O_2(g)$$

$$H_2O \text{ splitting: } CeO_{2-\delta_f} + (\delta_f - \delta_i)H_2O(g) \rightarrow CeO_{2-\delta_i} + (\delta_f - \delta_i)H_2(g)$$

$$CO_2 \text{ splitting: } CeO_{2-\delta_f} + (\delta_f - \delta_i)CO_2(g) \rightarrow CeO_{2-\delta_i} + (\delta_f - \delta_i)CO(g)$$

δ_i and δ_f represent initial and final oxygen nonstoichiometry within ceria, respectively. Reduction is typically operated at temperatures above 1300 °C and pO_2 between 10^{-4} and 10^{-8} atm releasing oxygen from metal oxide. Oxidation is usually operated at lower temperatures (i.e., $T < 800$ °C) and low pO_2 (i.e., $pO_2 < 10^{-14}$ atm); for higher temperatures (i.e., $T > 800$ °C), the pO_2 also has to increase (i.e., $pO_2 > 10^{-14}$ atm), leading to excess H_2O requirements.[1] The exact conditions depend on the thermodynamic properties of the oxide employed, and a thorough discussion can be found in the review by Carrillo and Scheffe.[2] During oxidation, the oxygen-deprived metal oxide reoxidizes with H_2O or CO_2 to generate synthesis gas such as H_2 or CO, which can be utilized as a fuel directly via combustion or transformed to liquid fuels, for example, via Fischer–Tropsch synthesis.[3,4]

Ceria is currently regarded as a state-of-the-art metal oxide because of its fast redox kinetics[1,5,6] and physical stability at high temperatures,[1,7] and it is easily oxidized over a wide range of oxidation conditions.[1] Ceria is extremely suitable for temperature-swing cycling, which is benefited by the large change in entropy that it undergoes as oxygen is released or incorporated into the solid; in general, the higher the partial molar entropy of the oxide, the higher the efficiency will be for a temperature-swing cycle.[8] The largest solar-to-fuel efficiency of 5.25% was recently measured using a porous ceria structure in a prototype solar reactor by Marxer et al.[9]

Received: August 25, 2020
Revised: October 28, 2020
Published: November 17, 2020

https://dx.doi.org/10.1021/acs.energyfuels.0c02872
Energy Fuels 2020, 34, 16918–16926

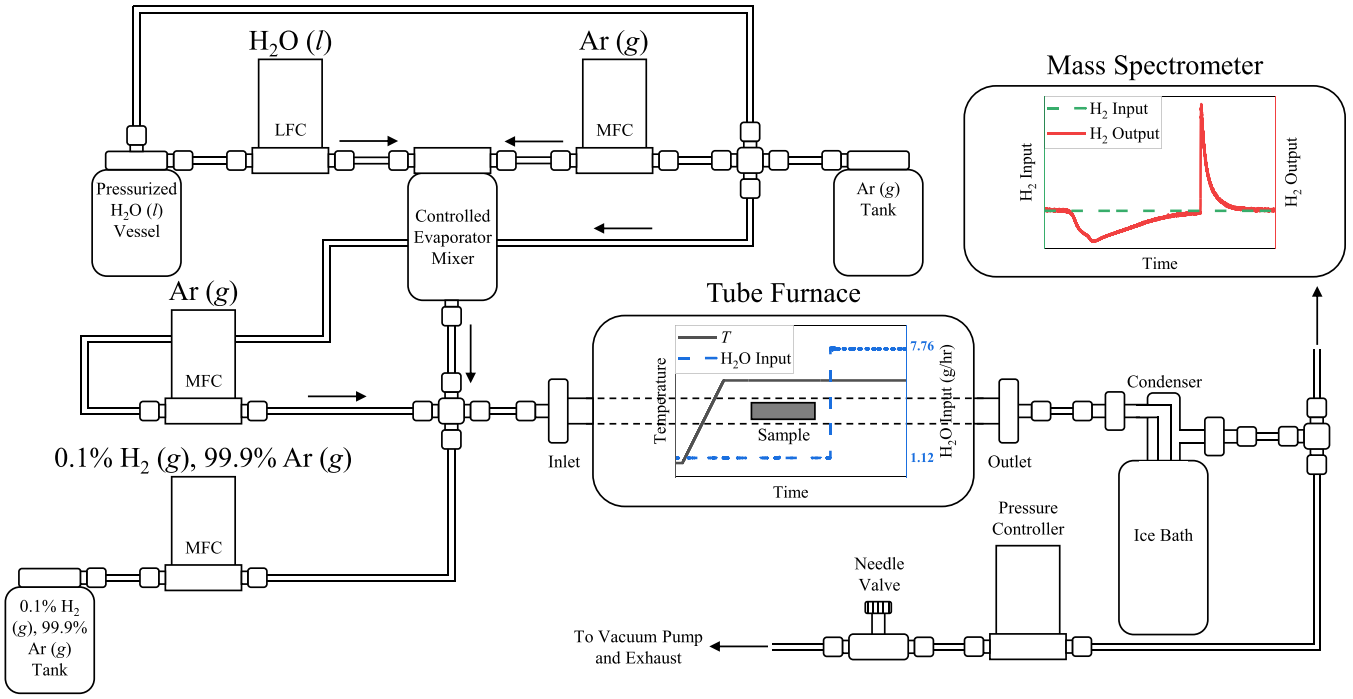

Figure 1. Schematic of the high-temperature tube furnace-based reactor system with exemplary H_2O and H_2 input, H_2 output, and corresponding temperature.

Solar-to-fuel efficiency for ceria increases as reduction temperature increases because of increased fuel yields, but limitations also arise at the same time, such as material degradation via sintering[1] or sublimation[10,11] and increasing radiative losses. Further, the sensible heating requirement of the solid is a major energy loss.[9,12] For example, according to Marxer et al. who measured the record efficiency, 63% of irreversibilities were because of solid heating caused by temperature-swing operation. Therefore, fuel production at lower operating temperatures and with smaller temperature swing, at the expense of increased heating demands of H_2O or CO_2, has been of interest in recent years because of the expected ease of gas-phase heat recuperation compared to the solid phase. Isothermal cycling of ceria has been studied via thermodynamic modeling[13−16] and experimentation.[17−19] Isothermal CO_2 splitting at 1500 °C in an IR imaging furnace was investigated by Venstrom et al.[17] who demonstrated 4% process efficiency using ceria with the assumption of 90% gas-phase heat recovery. Building on this work, isothermal CO_2 splitting in a 4.4 kW prototype reactor heated by a solar simulator was demonstrated by the same group.[18,19] The solar-to-fuel efficiency was 0.72% and 1.64% at 1750 K with and without consideration of the energy required to generate N_2 as a sweep gas during reduction, respectively. Although the efficiency using ceria was not as high as that of Marxer et al., this work established the viability of high-temperature gas-phase heat recuperation and demonstrated an effectiveness factor of 95%.

Perovskites with the ABO_3 structure are another class of well-documented candidates for thermochemical redox cycling, in part because of the tunable characteristics that various combinations of A-site and B-site dopants enable.[20] Lanthanum−strontium−manganese (LSM)-based perovskites have been widely investigated and regarded as promising candidate redox materials, especially at lower reaction temperatures compared to ceria.[21,22] For example, aluminum-doped LSM perovskites, such as $La_{0.6}Sr_{0.4}Mn_{0.6}Al_{0.4}O_3$ (LSMA6464), $La_{0.4}Sr_{0.6}Mn_{0.6}Al_{0.4}O_3$ (LSMA4664), and $La_{0.6}Sr_{0.4}Mn_{0.4}Al_{0.6}O_3$ (LSMA6446), were used to split H_2O and CO_2 in a stagnation flow reactor equipped with a near-infrared heating laser between 1350 and 1000 °C by McDaniel et al.[23] The amount of H_2 and CO produced under the same condition (reduced with 100 vol % He and oxidized with 40 vol % H_2O or CO_2) for all three LSMA perovskites was significantly higher than that of ceria. Extensive combinations of perovskites including La, Y, Sr, Ca, and Ba on the A-site and Mn, Al, Mg, Cr, Co, and Fe on the B-site were reviewed by Kubicek et al.[22] Overall, perovskites provide a very stable structure and accommodate a large oxygen vacancy concentration resulting in high fuel yields. All perovskites in the review were cycled at lower reduction temperatures, and 20 out of 42 perovskites afforded higher fuel yields than that of ceria. On the other hand, limitations of the perovskites were reported for temperature-swing cycling, such that oxidation of the perovskites are thermodynamically less favorable and they require large amounts of excess H_2O/CO_2 to obtain a higher fuel yield.[8,24] For example, LSM and LCM perovskite pellets with aluminum-doped on the B-site were investigated over a wide range of T (1573−1773 K) and pO_2 (9.9×10^{-5} to 4.5×10^{-2} bar) via thermogravimetric analysis and residual gas analysis by Takacs et al.[8] All perovskites reduced significantly more than ceria under the same T and pO_2, but H_2 yield of perovskites were higher than ceria only with excess H_2O/CO_2 and/or at lower oxidation temperatures. In general, changes in enthalpies and entropies of the perovskites were lower than that of ceria, which is the main reason that oxidation of the perovskites is less favorable than ceria.[25]

Isothermal cycling of perovskites has been demonstrated experimentally and, in general, they performed better compared to ceria. For example, isothermal CO_2 splitting of LSM30, LSM40, and LSM50 were demonstrated at 1673 K and 1773 K and compared to ceria by Dey and Rao.[26] The

https://dx.doi.org/10.1021/acs.energyfuels.0c02872
Energy Fuels 2020, 34, 16918−16926

Table 1. Experimental Conditions

	CERIA, LSM35			LSM40		
T (°C)	1300	1350	1400	1300	1350	1400
$pO_{2,red}$ (ATM)	8.87×10^{-7}	8.74×10^{-7}	8.65×10^{-7}	8.26×10^{-7}	8.13×10^{-7}	8.05×10^{-7}
$[nH_2O/nH_2]_{in,red}$	203.17	110.29	65.02	196.03	106.42	62.73
$[nH_2O/nH_2]_{in,ox1}$	507.93	507.93	507.93	490.08	490.08	490.08
$[nH_2O/nH_2]_{in,ox2}$	451.04	445.82	441.18	435.19	430.15	425.67
$[nH_2O/nH_2]_{in,ox3}$	309.40	271.09	260.06	298.53	261.56	250.92

amount of CO produced was higher for all LSM perovskites than ceria using 1 atm of pCO_2 during oxidation. Various combinations of Cr-doped LSM perovskites ($La_{0.6}Sr_{0.4}Cr_xMn_{1-x}O_3$, $0 \le x \le 0.85$) were investigated for isothermal CO_2 splitting in a high-temperature fixed-bed reactor and compared to ceria by Carrillo et al.[21] Peak CO production rate and CO yield for LSCM perovskites with $x \ge 0.5$ was higher than that of ceria at 1400 °C with 0.5 atm of pCO_2 during oxidation.

Our prior theoretical work explains why lanthanum−manganese-based perovskites have the potential for improved solar-to-fuel efficiencies compared to ceria in a high pO_2 region, where isothermal redox cycling is viable.[13] Isothermal cycling is viable here because oxidation has to be conducted at higher pO_2 than reduction during redox cycling; for temperature-swing cycling, it is oxidized at much lower pO_2 than reduction. In these high pO_2 regions (10^{-8} to 10^{-3} atm), ceria nonstoichiometry is relatively insensitive to changes in pO_2 compared to perovskite counterparts.[27−29] Because pO_2 is increased by increasing pH_2O in the system relative to pH_2, this means that larger changes in the oxidation state, and thus, greater H_2/CO yields are expected relative to the steam (or CO_2) input.

In this research, we aim to validate our theoretical predictions using a high-temperature tubular reactor system[30] to perform isothermal redox cycling of ceria and LSM-based perovskites, namely, $La_{0.65}Sr_{0.35}MnO_3$ (LSM35) and $La_{0.6}Sr_{0.4}MnO_3$ (LSM40), under controlled pH_2O/pH_2, where the redox reactions for LSM-based perovskites are as follows

$$\text{reduction: } La_{1-x}Sr_xMnO_{3-\delta_i} \rightarrow La_{1-x}Sr_xMnO_{3-\delta_f} + (\delta_f - \delta_i)/2O_2(g)$$

$$H_2O \text{ splitting: } La_{1-x}Sr_xMnO_{3-\delta_f} + (\delta_f - \delta_i)H_2O(g) \rightarrow La_{1-x}Sr_xMnO_{3-\delta_i} + (\delta_f - \delta_i)H_2(g)$$

Further, we introduce and substantiate a new metric, entitled performance (Π), that is defined as a function of easily measured properties that include $\Delta\delta$, oxidation temperature, and $[nH_2O/nH_2]_{in}$. We show that performance is proportional to the solar-to-fuel efficiency and compare the performance of the candidate materials over a range of isothermal conditions between 1300 and 1400 °C.

Experimental Methods. A schematic of the high temperature tube furnace reactor with exemplary H_2O input, H_2 output, and corresponding temperature profile is shown in Figure 1.[30] A tube furnace (Carbolite STF 16/180, 20−1600 °C) is utilized as the main heating source, which enables isothermal cycling up to 1600 °C with a maximum ramp rate of 20 °C/min. A 40 in.-long alumina (Al_2O_3) tube with an inner diameter of 0.75 in. is placed in the tube furnace to provide an indirect heat flux to the materials of interest and control the atmosphere. A boat crucible made of alumina with 2.75 in. length and 0.375 in. height is filled with powdered materials of interest and placed in the reaction tube at the center of the tube furnace. Two mass flow controllers (MKS Instruments, GE50A, 0−500 sccm) deliver Ar (99.999% purity) and 0.1% H_2 balanced Ar at the inlet of the system. A third mass flow controller (MKS Instruments, GE50A, 0−200 sccm) and a liquid flow controller (Bronkhorst, LIQUI-FLOW, 0−9 g/h) are connected to the controlled evaporator mixer (Bronkhorst, CEM Evaporator) that is heated at 200 °C and delivers H_2O vapor to the system. The alumina tube and all metal tubing that deliver gas into the system are heated by a heat tape, and the temperatures are controlled by three digital temperature controllers coupled with type-K thermocouples. An ice bath condenser is placed at the outlet of the alumina tube to prevent H_2O from condensing downstream near the sample capillary of the mass spectrometer. Total pressure is controlled to 1 atm by a pressure controller (MKS Instruments, type 640B) and a vacuum pump (Edwards, E2M0.7) that are placed downstream of the condenser. A mass spectrometer (Stanford Research Systems, QMS100) is connected at the outlet of the condenser to sample the gas species.

Two gram of commercially available ceria powder (Alfa Aesar) and LSM35 powder (Nexceris LLC) and 2 g of LSM40 powder that was synthesized using the modified Pechini method in-house[31,32] were prepared and tested. Procedures and details for the synthesis technique are described in prior work for yttrium−strontium−manganese-based perovskites.[33] For LSM40, $La(NO_3)_3{\cdot}6H_2O$ (Sigma-Aldrich) was used instead of $Y(NO_3)_3{\cdot}6H_2O$ and no $Al(NO_3)_3{\cdot}9H_2O$ was used, and the X-ray diffraction (XRD) patterns after the synthesis is shown in Figure S1 with comparison to literature. The LSM35 powder used here is 5% A-site deficient, as specified by the manufacturer.

All redox cycling was performed using 400 sccm of 100% Ar, continuously balanced with 200 sccm of 0.1% H_2 in Ar, with variable amounts of H_2O (depending on the desired pO_2), as described further below. This H_2O and H_2 mixture was used during reduction and oxidation so that we could have precise control of the pO_2, as we have shown in a prior work.[30] The relevant equation to calculate pO_2 from the pH_2O, pH_2, and the equilibrium constant of water dissociation (K_w) is shown as follows

$$K_w = \frac{pH_2 \cdot (pO_2)^{0.5}}{pH_2O}$$

H_2 was calibrated prior to each experiment using the measured flowrates of H_2 and Ar from the flow controllers and the partial pressures of H_2 and Ar from the mass spectrometer. Following calibration, the temperature of the furnace was increased from ambient to either 200 or 300 °C. Once this set

https://dx.doi.org/10.1021/acs.energyfuels.0c02872
Energy Fuels 2020, 34, 16918−16926

point was achieved, liquid H_2O was delivered at either 3.5, 1.9, or 1.12 g/h for experiments at 1300, 1350, and 1400 °C, respectively. These liquid flowrates were used to ensure that the pO_2 during reduction in each experiment was as consistent as possible near 8.5×10^{-7} atm. Temperature ramping to the target temperatures began 30 min after the initial H_2O delivery at a ramp rate of 20 °C/min. During heating to one of the three set point temperatures, reduction was initiated and an appropriate amount of time was given at the set point to allow the system to approach an equilibrium. Following this, the liquid flow rate of H_2O was increased to initiate oxidation. Subsequent isothermal cycling was repeated by maintaining the constant flow rate of H_2, while changing the flow rate of H_2O to increase or decrease the pO_2. The experimental conditions investigated for each material are shown in Table 1. Nonstoichiometry after the first reduction (δ_{red}) was calculated by integrating the area of the molar H_2 flow rate with time with respect to the set baseline during the first reduction, assuming that the sample started at $\delta = 0$. H_2 yield was calculated by integrating the subsequent areas of the molar H_2 flow rate with time during oxidation and reduction, ensuring that the mass balance is closed for every cycle. Three isothermal conditions per temperature were performed for each material, with multiple repetitions for each experiment to ensure repeatability. Here, $[nH_2O/nH_2]_{in,red}$ represents the molar ratio of H_2O to H_2 input during the first reduction, $[nH_2O/nH_2]_{in,ox1}$ represents the molar ratio of H_2O to H_2 input during the first oxidation, and so on.

RESULTS AND DISCUSSION

Isothermal Cycling of Ceria, LSM35, and LSM40. H_2 molar flowrate, corresponding H_2O input, and the temperature profile of ceria during isothermal cycling at 1400 °C are shown in Figure 2. During heating, reduction begins near 600 °C

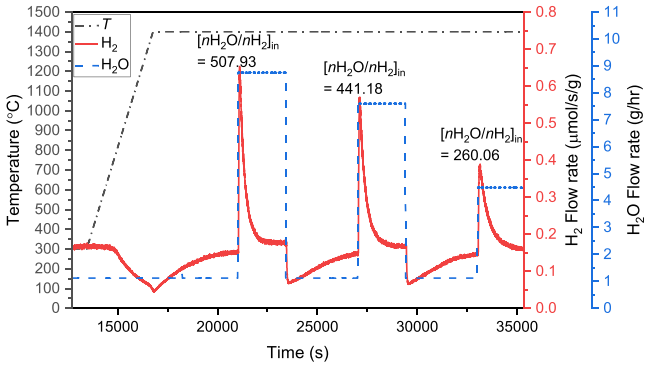

Figure 2. H_2 production and consumption during the isothermal cycling of ceria at 1400 °C and corresponding H_2O input and temperature profile.

resulting in consumption of H_2 and a decrease in H_2 flow rate until the temperature reaches 1400 °C. Afterward, it increases back to baseline: δ_{red} was estimated to be 0.052. Oxidation was then initiated by increasing the H_2O flow rate to 8.75 g/h, corresponding to $[nH_2O/nH_2]_{in}$ = 507.93. The reaction rate increased rapidly during the first 50 s until it peaked at 0.65 μmol/s/g, and it decreased slowly until it reached the baseline. The calculated H_2 yield and $\Delta\delta$ for the first oxidation was 166.22 and 0.029 μmol/g, respectively. The second reduction was initiated by a decrease in the H_2O flow rate from 8.75 to 1.12 g/h, corresponding to $[nH_2O/nH_2]_{in,red}$ = 65.02. The H_2 consumption yield and $\Delta\delta$ here equaled 173.53 and 0.030 μmol/g, respectively, confirming that the mass balance was closed. This was consistent for all experiments performed. The second and third cycles were performed in a similar procedure, albeit with lower $[nH_2O/nH_2]_{in}$, resulting in H_2 yields during oxidation of 161.79 and 127.86 μmol/g, respectively. H_2 consumption yields during the second and third reduction were 173.53 and 153.82 μmol/g, respectively. H_2 consumption yield was not measured after the last oxidation of each set of the experiment.

H_2 molar flowrate, corresponding H_2O input, and the temperature profile of LSM40 during isothermal cycling at 1400 °C are shown in Figure 3. The first reduction began at a

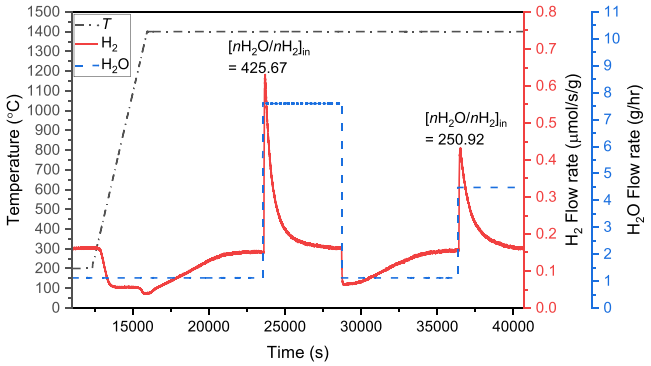

Figure 3. H_2 production and consumption during the isothermal cycling of LSM40 at 1400 °C and corresponding H_2O input and temperature profile.

lower temperature compared to ceria, and there was an obvious change in the reaction rate near 600 °C, where it leveled off for an extended period of time. This change in the reaction rate is potentially related to the plateaus at $\delta = 0.0225$ in δ *versus* pO_2 curve of LSM40, as reported by Mizusaki et al.[28,29] The distribution of oxygen vacancies on the oxygen sublattice is different for $\delta > 0.0225$ and for $\delta < 0.0225$. In general, the trends observed for LSM40 are very similar to ceria, except for the noticeable increase in reaction times during reduction and oxidation. This is because the reaction extents for LSM40 were substantially greater. For example, the H_2 yield during the first cycle with LSM40 is 383.30 μmol/g, compared to 166.22 μmol/g for ceria, even though the pO_2, or $[nH_2O/nH_2]_{in}$, is lower. The isothermal cycling of LSM35 was performed very similarly to that of LSM40 and, in general, the results appear qualitatively similar and are thus not shown here. However, temporal results for all samples and temperatures are shown in Figures S2–S14, and yields are summarized in the subsequent section.

H_2 Yield of Ceria, LSM35, and LSM40. For all conditions that were investigated, LSM35 and LSM40 outperform ceria in terms of H_2 yield. A summary of H_2 yield and $\Delta\delta$ as a function of $[nH_2O/nH_2]_{in}$ at 1300, 1350, and 1400 °C is shown in Figure 4a–c, respectively, for each material. The measured initial reduction extents for ceria, LSM35, and LSM40 at 1300, 1350, and 1400 °C are summarized in Table 2. Both LSM35 and LSM40 have steeper slopes and greater H_2 yield for all $[nH_2O/nH_2]_{in}$ compared to ceria, indicating that LSM35 and LSM40 perform better isothermally because they require less H_2O to oxidize per mole of H_2 produced. The implication of these results is further explained in the following section. Also included (but not distinguished) in the data points shown is

https://dx.doi.org/10.1021/acs.energyfuels.0c02872
Energy Fuels 2020, 34, 16918–16926

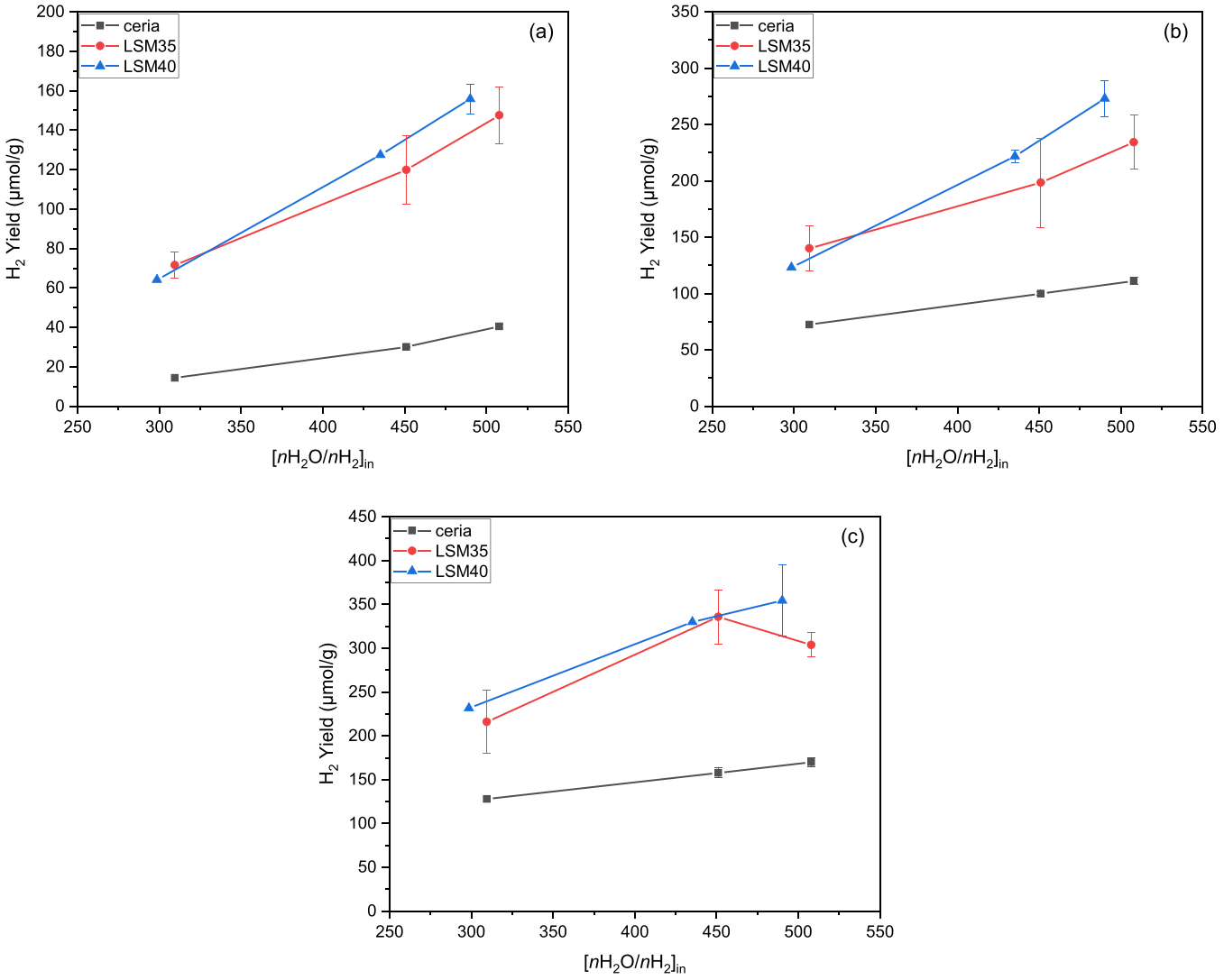

Figure 4. H_2 yield per gram of ceria, LSM35, and LSM40 *vs* $[nH_2O/nH_2]_{in}$, (a) at 1300, (b) at 1350, and (c) at 1400 °C.

Table 2. Measured Reduction Extents of Ceria, LSM35, and LSM40 at Various Temperatures

T (°C)	1300	1350	1400
$\delta_{red,ceria}$	0.025	0.035	0.052
$\delta_{red,LSM35}$	0.092 ± 0.004	0.115 ± 0.009	0.131 ± 0.012
$\delta_{red,LSM40}$	0.087	0.123	0.144

H_2 consumption during reduction following each oxidation, which helps to provide more confidence in the experimental error. For example, the H_2 consumed going from high to low pO_2 should be equal to H_2 produced during the prior oxidation when the pO_2 goes in the reverse direction. Regarding the apparent decrease in yield for high $[nH_2O/nH_2]_{in}$ for LSM35, as shown in Figure 4c, we attribute this to experimental variability, as evidenced by the large error bars for the point immediately adjacent at lower $[nH_2O/nH_2]_{in}$.

A summary of H_2 yields for ceria, LSM40, and LSM35 with a comparison to the available literature data is shown in Figures 5−7, respectively. Literature predictions were made from the experimentally derived thermodynamic data, namely, partial molar enthalpy and entropy, which were used to predict δ as a function of T and pO_2.[27−29] Data for ceria are compared using data from Panlener et al.,[27] data for LSM40 are compared

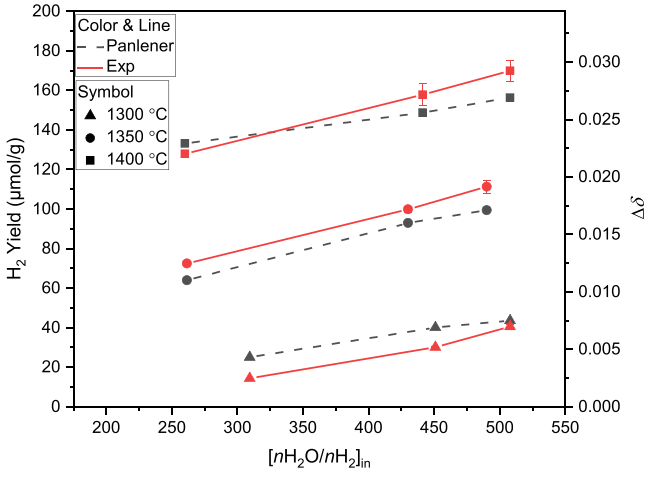

Figure 5. H_2 yield per gram of ceria and corresponding $\Delta\delta$ *vs* $[nH_2O/nH_2]_{in}$ at 1300, 1350, and 1400 °C and comparison to Panlener et al. Red solid line and black dashed line represent our data and thermodynamic predictions from Panlener et al., respectively.

using data from Mizusaki et al.,[28] and data for LSM35 are compared to data of LSM30 and LSM40 from Mizusaki et

https://dx.doi.org/10.1021/acs.energyfuels.0c02872
Energy Fuels 2020, 34, 16918−16926

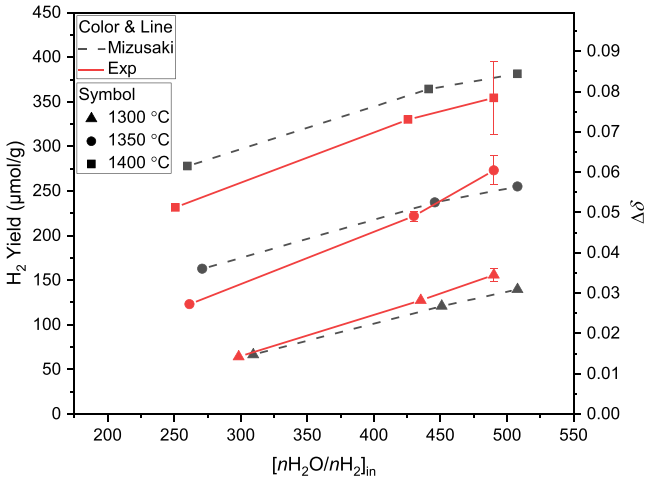

Figure 6. H_2 yield per gram of LSM40 and corresponding $\Delta\delta$ *vs* $[nH_2O/nH_2]_{in}$ at 1300, 1350, and 1400 °C and comparison to Mizusaki et al. Red solid line and black dashed line represent our data and thermodynamic predictions from Mizusaki et al., respectively.

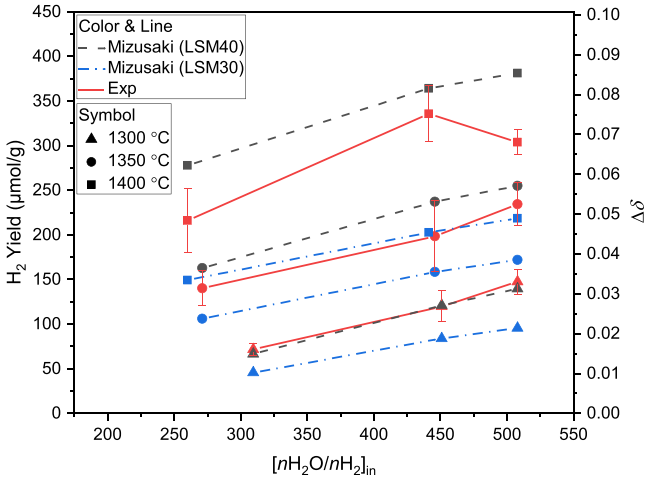

Figure 7. H_2 yield per gram of LSM35 and corresponding $\Delta\delta$ *vs* $[nH_2O/nH_2]_{in}$ at 1300, 1350, and 1400 °C and comparison to Mizusaki et al. Red solid line represents our data, and black dashed and blue dash-dot lines represent LSM40 and LSM30 from Mizusaki et al., respectively.

al.[28,29] For each material, measured H_2 yield increases with the increase in temperature, primarily because the reduction extent increases with increasing temperature while keeping pO_2 constant. This results in a greater capacity for oxidation, even at the expense of increasing temperature which negatively impacts oxidation performance. Overall, the experimental data are close to the predicted values based on Panlener et al. and Mizusaki et al. LSM35 data fall between LSM30 and LSM40 from Mizusaki et al., also as expected, except at 1300 °C when they are very close to LSM40. This is possibly because the LSM35 used here is A-site deficient, while LSM30 and LSM40 are not, and the difference between the data points for LSM40 and LSM30 is relatively small to begin with at these conditions.

Performance of Ceria, LSM35, and LSM40. A general metric of comparison, called performance (Π), is presented to compare material suitability for isothermal cycling directly and easily from experimental data points similar to those measured in this work (i.e., H_2 yield or $\Delta\delta$ as a function of $[nH_2O/nH_2]_{in}$). The metric is designed to be computed measuring only $\Delta\delta$ as a function of temperature and $[nH_2O/nH_2]_{in}$ and is proportional to solar-to-fuel efficiency; it can be applied to isothermal, near isothermal, and temperature-swing cycling, but in this analysis, it is only used for isothermal comparison. Π is defined below, where $C_{p,s}$ is the specific heat of the solid material, ΔT is the magnitude of the temperature-swing, T_{ox} is the oxidizing temperature, and C_{p,H_2O} is the gas-phase specific heat of H_2O which is assumed to be constant.

$$\Pi = \frac{\Delta\delta}{(C_{p,s}\cdot\Delta T) + [[nH_2O/nH_2]_{in,ox}\cdot T_{ox}\cdot C_{p,H_2O}]}$$

The solar-to-fuel efficiency is defined below, where HHV_{H_2} is the higher heating value of H_2, $\Delta H_{H_2O}|_{298K\text{-}TL}$ is the enthalpy required to heat H_2O from 298 K to T_L, HR is the fraction of heat recuperated, ΔH_{red} is the reduction enthalpy, δ is the reduction extent, and $\eta_{absorption}$ is the solar energy absorption efficiency.[34]

$$\eta_{solar\text{-}to\text{-}fuel} = \frac{HHV_{H_2}\cdot nH_2}{\left\{\left[\Delta H_{H_2O}|_{298K\rightarrow T_L}\cdot nH_2O + \int_{T_L}^{T_H} C_{p,s}\,dT\right]\times(1-HR) + \Delta H_{red}\cdot\delta\right\}/\eta_{absorption}}$$

As seen, this definition of Π is closely related to the efficiency equation,[34] but the heating value of H_2 is removed from the numerator, constant specific heats are used, and nH_2 is included in the denominator. For isothermal cycling, the bottom left term containing ΔT equals 0, and T_{ox} is the operating temperature for the entire cycle. The oxidation ratio, $[nH_2O/nH_2]_{in}$, is directly related to the required steam input to achieve a given H_2 yield. This equation captures the importance of the slope of the isotherms in the H_2 yield *versus* $[nH_2O/nH_2]_{in}$ plots presented in this study. The most desirable material is the one which achieves a large change in oxygen nonstoichiometry as a result of a minimal shift in $[nH_2O/nH_2]_{in}$. For example, a material with a steep isotherm within this space introduced to a small amount of steam will produce more H_2 than that of a material with a shallow slope. The material with the steeper slope will have a higher performance and thus a higher solar-to-fuel efficiency because of the lower amount of required steam input and consequently less sensible energy input to heat H_2O to the operating temperature.

In the preceding section, it was shown that the slope of the H_2 yield *versus* $[nH_2O/nH_2]_{in}$ plots for LSM35 and LSM40 were steeper than ceria. The relationship between these results and Π is shown in Figure 8, where Π is shown for LSM40, LSM35, and ceria as a function of $[nH_2O/nH_2]_{in}$; materials were reduced at 1300 °C and $[nH_2O/nH_2]_{in,red} = 203$, or $pO_2 = 8.87 \times 10^{-7}$ atm. The smooth solid and dashed lines represent predicted values for performance and H_2 yield calculated from the aforementioned thermodynamic data of Mizusaki et al.[28,29] and Panlener et al.;[27] here, data are smooth because $\Delta\delta$ was calculated with small increases in $[nH_2O/nH_2]_{in}$. Dotted dashed lines represent our experimental data, where diamonds represent Π and asterisks represent H_2 yield. As expected, LSM40 and LSM35 display higher performances than ceria. These results agree well with Carrillo's theoretical comparison of efficiency between ceria and several perovskites including LSM40,[13] where LSM40 was shown to be more

https://dx.doi.org/10.1021/acs.energyfuels.0c02872
Energy Fuels 2020, 34, 16918−16926

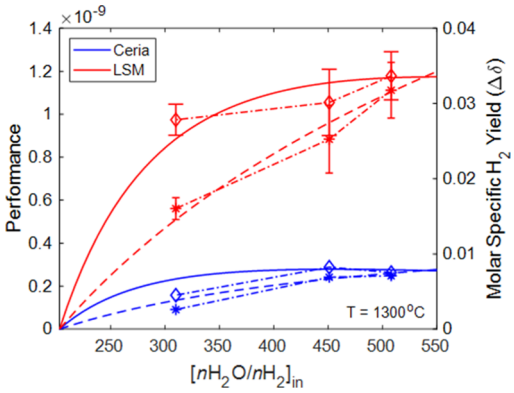

Figure 8. Π and molar specific H_2 yield as a function of $[nH_2O/nH_2]_{in}$ at 1300 °C, reduced at $[nH_2O/nH_2]_{in,red}$ of 203, or $pO_2 = 8.87 \times 10^{-7}$ atm. The smooth solid and dashed lines represent predicted values for performance and H_2 yield calculated from Panlener et al. and Mizusaki et al., respectively. Dotted dashed lines represent our experimental data, where diamonds represent Π and asterisks represent H_2 yield.

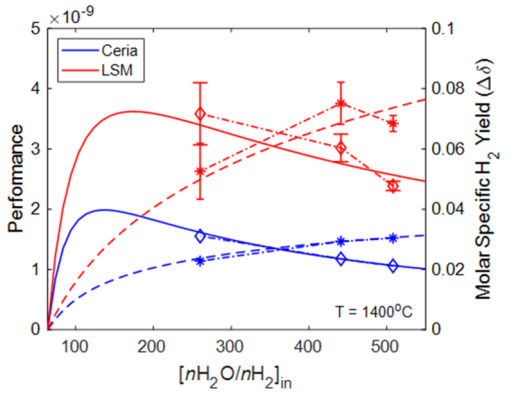

Figure 10. Π and molar specific H_2 yield as a function of $[nH_2O/nH_2]_{in}$ at 1400 °C, reduced at $[nH_2O/nH_2]_{in,red}$ of 65, or $pO_2 = 8.65 \times 10^{-7}$ atm. The smooth solid and dashed lines represent predicted values for performance and H_2 yield calculated from Panlener et al. and Mizusaki et al. Dotted dashed lines represent our experimental data, where diamonds represent Π and asterisks represent H_2 yield.

efficient under similar conditions as described in the prior sections. Results for isothermal operation at 1350 and 1400 °C are shown in Figures 9 and 10, respectively. In these cases, Π

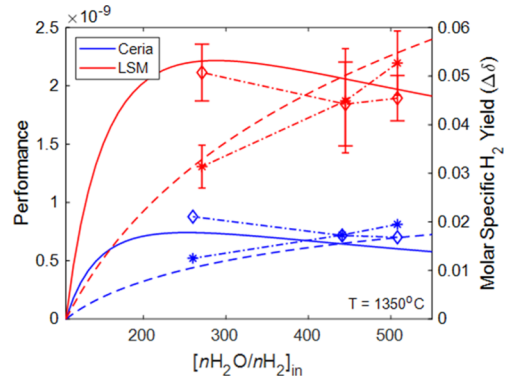

Figure 9. Π and molar specific H_2 yield as a function of $[nH_2O/nH_2]_{in}$ at 1350 °C, reduced at $[nH_2O/nH_2]_{in,red}$ of 106, or $pO_2 = 8.13 \times 10^{-7}$ atm. The smooth solid and dashed lines represent predicted values for performance and H_2 yield calculated from Panlener et al. and Mizusaki et al., respectively. Dotted dashed lines represent our experimental data, where diamonds represent Π and asterisks represent H_2 yield.

shows notable peaks at an intermediate $[nH_2O/nH_2]_{in}$, even as $\Delta\delta$ continues to increase. This is because as temperature increases, pO_2 also increases and the materials are more readily oxidized at a fixed $[nH_2O/nH_2]_{in}$: further increases result in diminishing H_2 yields that are not compensated by the extra H_2O required to obtain them. Further, Π increases overall with increasing temperature, but it should be noted that radiative losses are not accounted for in this definition and the decrease with increasing $[nH_2O/nH_2]_{in}$ is more pronounced as temperature increases.

CONCLUSIONS

This work presents a fair comparison between ceria and LSM perovskites for isothermal redox cycling via a controlled $[nH_2O/nH_2]_{in}$ at temperatures between 1300 and 1400 °C. A new metric of performance was introduced and is effective in comparing the fuel yield at a given range of T and $[nH_2O/nH_2]_{in}$ and thus provides the suitability of a candidate redox material under the given experimental conditions. Overall, we observed that LSM35 and LSM40 significantly outperformed ceria in terms of H_2 yield and Π with steeper slopes of H_2 yield *versus* $[nH_2O/nH_2]_{in}$ for all experimental conditions, indicating that more H_2 is produced with the same amount of H_2O input. Π captures the importance of the slope of the isotherms in H_2 yield *versus* $[nH_2O/nH_2]_{in}$ and thus provides a straightforward comparison among materials without a need to calculate efficiency. The experimental data were validated by comparing to the literature, and they agree well with the thermodynamic predictions that the LSM perovskites can undergo larger $\Delta\delta$ and higher performance, or solar-to-fuel efficiency, compared to ceria in high pO_2 conditions, where isothermal cycling is conducted. This work adds motivation for further material development and exploration beyond materials with large entropic changes during redox cycling, but also for materials that undergo large $\Delta\delta$ in the high pO_2 range between 10^{-8} and 10^{-3} atm where isothermal or near isothermal redox cycles are most viable.

ASSOCIATED CONTENT

Supporting Information

The Supporting Information is available free of charge at https://pubs.acs.org/doi/10.1021/acs.energyfuels.0c02872.

Comparison of the XRD patterns of the fresh LSM40 powder to the literature and H_2 production and consumption during the isothermal cycling of ceria, LSM35, and LSM40 at 1300, 1350, and 1400 °C with corresponding H_2O input and temperature profile (PDF)

AUTHOR INFORMATION

Corresponding Author

Jonathan R. Scheffe − *Department of Mechanical and Aerospace Engineering, University of Florida, Gainesville, Florida 32611-6250, United States*; Email: jscheffe@ufl.edu

Authors

Kangjae Lee − *Department of Mechanical and Aerospace Engineering, University of Florida, Gainesville, Florida*

https://dx.doi.org/10.1021/acs.energyfuels.0c02872
Energy Fuels 2020, 34, 16918−16926

32611-6250, United States; orcid.org/0000-0002-2494-2372

Dylan C. McCord − *Department of Mechanical and Aerospace Engineering, University of Florida, Gainesville, Florida 32611-6250, United States*

Richard J. Carrillo − *Department of Mechanical and Aerospace Engineering, University of Florida, Gainesville, Florida 32611-6250, United States*

Bella Guyll − *Department of Mechanical Engineering, Iowa State University, Ames, Iowa 50011-2030, United States*

Complete contact information is available at: https://pubs.acs.org/10.1021/acs.energyfuels.0c02872

Notes

The authors declare no competing financial interest.

■ ACKNOWLEDGMENTS

We gratefully acknowledge financial support from the U.S. Department of Energy Fuel Cell Technology Office (award number: DE-EE0008840), the NSF REU program (award number: 1757128), and the University of Florida's College of Engineering and Department of Mechanical and Aerospace Engineering.

■ REFERENCES

(1) Chueh, W. C.; Haile, S. M. A thermochemical study of ceria: exploiting an old material for new modes of energy conversion and CO2 mitigation. *Philos. Trans. R. Soc., A* **2010**, *368*, 3269−3294.

(2) Carrillo, R. J.; Scheffe, J. R. Advances and trends in redox materials for solar thermochemical fuel production. *Sol. Energy* **2017**, *156*, 3−20.

(3) Schulz, H. Short history and present trends of Fischer-Tropsch synthesis. *Appl. Catal., A* **1999**, *186*, 3−12.

(4) Riedel, T.; Schulz, H.; Schaub, G.; Jun, K.-W.; Hwang, J.-S.; Lee, K.-W. Fischer-Tropsch on iron with H-2/CO and H-2/CO2 as synthesis gases: the episodes of formation of the Fischer-Tropsch regime and construction of the catalyst. *Top. Catal.* **2003**, *26*, 41−54.

(5) Chueh, W. C.; Haile, S. M. Ceria as a Thermochemical Reaction Medium for Selectively Generating Syngas or Methane from H2O and CO2. *Chemsuschem* **2009**, *2*, 735−739.

(6) Ackermann, S.; Scheffe, J. R.; Steinfeld, A. Diffusion of Oxygen in Ceria at Elevated Temperatures and Its Application to H2O/CO2 Splitting Thermochemical Redox Cycles. *J. Phys. Chem. C* **2014**, *118*, 5216−5225.

(7) Toft Sørensen, O. Thermodynamic Studies Of Phase Relationships Of Nonstoichiometric Cerium Oxides At Higher Temperatures. *J. Solid State Chem.* **1976**, *18*, 217−233.

(8) Takacs, M.; Hoes, M.; Caduff, M.; Cooper, T.; Scheffe, J. R.; Steinfeld, A. Oxygen nonstoichiometry, defect equilibria, and thermodynamic characterization of LaMnO3 perovskites with Ca/Sr A-site and Al B-site doping. *Acta Mater.* **2016**, *103*, 700−710.

(9) Marxer, D.; Furler, P.; Takacs, M.; Steinfeld, A. Solar thermochemical splitting of CO2 into separate streams of CO and O-2 with high selectivity, stability, conversion, and efficiency. *Energy Environ. Sci.* **2017**, *10*, 1142−1149.

(10) Furler, P.; Scheffe, J.; Gorbar, M.; Moes, L.; Vogt, U.; Steinfeld, A. Solar Thermochemical CO2 Splitting Utilizing a Reticulated Porous Ceria Redox System. *Energy Fuels* **2012**, *26*, 7051−7059.

(11) Furler, P.; Scheffe, J. R.; Steinfeld, A. Syngas production by simultaneous splitting of H2O and CO2 via ceria redox reactions in a high-temperature solar reactor. *Energy Environ. Sci.* **2012**, *5*, 6098−6103.

(12) Siegrist, S.; von Storch, H.; Roeb, M.; Sattler, C. Moving Brick Receiver-Reactor: A Solar Thermochemical Reactor and Process Design With a Solid-Solid Heat Exchanger and On-Demand Production of Hydrogen and/or Carbon Monoxide. *J. Sol. Energy Eng.* **2019**, *141*, 021009.

(13) Carrillo, R. J.; Scheffe, J. R. Beyond Ceria: Theoretical Investigation of Isothermal and Near Isothermal Redox Cycling of Perovskites for Solar Thermochemical Fuel Production. *Energy Fuels* **2019**, *33*, 12871−12884.

(14) Bader, R.; Venstrom, L. J.; Davidson, J. H.; Lipiński, W. Thermodynamic Analysis of Isothermal Redox Cycling of Ceria for Solar Fuel Production. *Energy Fuels* **2013**, *27*, 5533−5544.

(15) Lin, M.; Haussener, S. Solar fuel processing efficiency for ceria redox cycling using alternative oxygen partial pressure reduction methods. *Energy* **2015**, *88*, 667−679.

(16) Hao, Y.; Jin, J.; Jin, H. Thermodynamic analysis of isothermal CO2 splitting and CO2-H2O co-splitting for solar fuel production. *Appl. Therm. Eng.* **2020**, *166*, 113600.

(17) Venstrom, L. J.; De Smith, R. M.; Hao, Y.; Haile, S. M.; Davidson, J. H. Efficient Splitting of CO2 in an Isothermal Redox Cycle Based on Ceria. *Energy Fuels* **2014**, *28*, 2732−2742.

(18) Hathaway, B. J.; Bala Chandran, R.; Gladen, A. C.; Chase, T. R.; Davidson, J. H. Demonstration of a Solar Reactor for Carbon Dioxide Splitting via the Isothermal Ceria Redox Cycle and Practical Implications. *Energy Fuels* **2016**, *30*, 6654−6661.

(19) Hathaway, B. J.; Chandran, R.; Sedler, S.; Thomas, D.; Gladen, A.; Chase, T.; Davidson, J. Effect of Flow Rates on Operation of a Solar Thermochemical Reactor for Splitting CO2 Via the Isothermal Ceria Redox Cycle. *J. Sol. Energy Eng.* **2016**, *138*, 011007.

(20) Muhich, C. L.; Blaser, S.; Hoes, M. C.; Steinfeld, A. Comparing the solar-to-fuel energy conversion efficiency of ceria and perovskite based thermochemical redox cycles for splitting H2O and CO2. *Int. J. Hydrogen Energy* **2018**, *43*, 18814−18831.

(21) Carrillo, A. J.; Bork, A.; Moser, T.; Sediva, E.; Hood, Z.; Rupp, J. Modifying La0.6Sr0.4MnO3 Perovskites with Cr Incorporation for Fast Isothermal CO2-Splitting Kinetics in Solar-Driven Thermochemical Cycles. *Adv. Energy Mater.* **2019**, *9*, 1803886.

(22) Kubicek, M.; Bork, A. H.; Rupp, J. L. M. Perovskite oxides - a review on a versatile material class for solar-to-fuel conversion processes. *J. Mater. Chem. A* **2017**, *5*, 11983−12000.

(23) McDaniel, A. H.; Miller, E. C.; Arifin, D.; Ambrosini, A.; Coker, E. N.; O'Hayre, R.; Chueh, W. C.; Tong, J. Sr- and Mn-doped LaAlO3-delta for solar thermochemical H-2 and CO production. *Energy Environ. Sci.* **2013**, *6*, 2424−2428.

(24) Scheffe, J. R.; Weibel, D.; Steinfeld, A. Lanthanum-Strontium-Manganese Perovskites as Redox Materials for Solar Thermochemical Splitting of H2O and CO2. *Energy Fuels* **2013**, *27*, 4250−4257.

(25) Scheffe, J. R.; Steinfeld, A. Oxygen exchange materials for solar thermochemical splitting of H2O and CO2: a review. *Mater. Today* **2014**, *17*, 341−348.

(26) Dey, S.; Rao, C. N. R. Splitting of CO2 by Manganite Perovskites to Generate CO by Solar Isothermal Redox Cycling. *ACS Energy Lett.* **2016**, *1*, 237−243.

(27) Panlener, R. J.; Blumenthal, R. N.; Garnier, J. E. A thermodynamic study of nonstoichiometric cerium dioxide. *J. Phys. Chem. Solids* **1975**, *36*, 1213−1222.

(28) Mizusaki, J.; Tagawa, H.; Naraya, K.; Sasamoto, T. Nonstoichiometry and thermochemical stability of the perovskite-type La1−xSrxMnO3−δ. *Solid State Ionics* **1991**, *49*, 111−118.

(29) Mizusaki, J.; Mori, N.; Takai, H.; Yonemura, Y.; Minamiue, H.; Tagawa, H.; Dokiya, M.; Inaba, H.; Naraya, K.; Sasamoto, T.; Hashimoto, T. Oxygen nonstoichiometry and defect equilibrium in the perovskite-type oxides La1-xSrxMnO3+d. *Solid State Ionics* **2000**, *129*, 163−177.

(30) Carrillo, R. J.; Warren, K.; Scheffe, J. Experimental Framework for Evaluation of the Thermodynamic and Kinetic Parameters of Metal-Oxides for Solar Thermochemical Fuel Production. *J. Sol. Energy Eng.* **2019**, *141*, 021007.

(31) Pechini, M. P. Method of preparing lead and alkaline earth titanates and niobates and coating method using the same to form a capacitor. U.S. Patent 3,330,697 A, 1967.

(32) Cooper, T.; Scheffe, J. R.; Galvez, M. E.; Jacot, R.; Patzke, G.; Steinfeld, A. Lanthanum Manganite Perovskites with Ca/Sr A-site and Al B-site Doping as Effective Oxygen Exchange Materials for Solar Thermochemical Fuel Production. *Energy Technol.* **2015**, *3*, 1130−1142.
(33) Carrillo, R. J.; Hill, C. M.; Warren, K. J.; Scheffe, J. R. Oxygen Nonstoichiometry and Defect Equilibria of Yttrium Manganite Perovskites with Strontium A-Site and Aluminum B-Site Doping. *J. Phys. Chem. C* **2020**, *124*, 4448−4458.
(34) Scheffe, J. R.; Steinfeld, A. Thermodynamic Analysis of Cerium-Based Oxides for Solar Thermochemical Fuel Production. *Energy Fuels* **2012**, *26*, 1928−1936.

https://dx.doi.org/10.1021/acs.energyfuels.0c02872
Energy Fuels 2020, 34, 16918−16926